Effects of microbubbles on removal of viscous oil adhering to channel wall

Li, Yuegui
Hayashi, Kosuke
Okamoto, Fuyuki
Hosokawa, Shigeo
Tomiyama, Akio

(Citation)
Chemical Engineering Research and Design,193:75-84

(Issue Date)
2023-05

(Resource Type)
journal article

(Version)
Accepted Manuscript

Effects of Microbubbles on Removal of Viscous Oil Adhering to Channel Wall

Yuegui Li[a], Kosuke Hayashi[a]*, Fuyuki Okamoto[a], Shigeo Hosokawa[b], Akio Tomiyama[a]

[a] Department of Mechanical Engineering, Graduate School of Engineering, Kobe University, 1-1 Rokkodai, Nada, Kobe 657-8501, Japan

[b] Faculty of Societal Safety Science, Kansai University, 7-1 Hakubai, Takatsuki, Osaka 569-1098, Japan

Abstract

It has been reported that the addition of microbubbles in a water flow enhances a cleaning efficiency of oil adhering to a channel wall. However, the enhancement mechanism of the cleaning effect has not been sufficiently understood yet. Experiments on the removal effects of water flows in a horizontal channel with and without microbubbles were therefore conducted to investigate the removal process by microbubbles. Silicone oil adhering to the bottom wall of the channel was used as dirt. The local thickness of the oil was measured during cleaning from micrographs of fluorescence intensity. The amount of oil removed by the water flow increased with increasing the Reynolds number. Adding microbubbles to the water flow increased the amount of removed oil. Microbubbles attached to the oil interface under turbulent conditions, and the bubbles grew by mass transfer through the gas-liquid interface and bubble coalescence. The detachment of bubbles grown on the oil interface led to oil peel-off, resulting in an improvement of cleaning effect.

Keywords: *Cleaning, Oil removal, Bubble diameter, Bubble number density*

Nomenclature

T	temperature [K]
DO	dissolved oxygen concentration [kg/m^3]
Q	liquid volume flow rate [m^3/s]
d_H	hydraulic equivalent diameter [m]
S	measurement area [m^2]
S_c	channel cross-sectional area [m^2]
P_e	perimeter of the channel [m]
Re	Reynolds number [-]
I	fluorescence intensity [-]
M	mask function [-]
C	concentration of fluorescent dye [mol/L]
I_L	intensity of laser light [-]
I_P	intensity for photobleaching without flow [-]
I_C	intensity under cleaning [-]
d_B	sphere-volume-equivalent bubble diameter [μm]
n_B	number density [m^{-3}]
N_B	number of bubble [-]
K	number of sample image [-]
u^*	frictional velocity [m/s]
c_s	dimensionless constant for shear-induced oil removal [-]
c_B	constant for oil removal by microbubble [m^3/s]
L	distance from oil interface [m]
t	time [s]
t'	time for bubble growth [s]

Greek letters

δ	oil thickness [μm]
u	cross-sectional mean velocity [m/s]
ρ	density [kg/m^3]
μ	viscosity [Pa·s]
τ_w	shear stress [Pa]

Subscripts

H	hydraulic equivalent
c	channel

e	wetting/equal diameter
L	laser
P	photobleaching
C	cleaning
B	bubble
w	water

1. Introduction

Microbubbles of 1-100 μm in diameter [1] are characterized by high internal pressure and long residence time [2] and have been reported to have cleaning effects [3] and to reduce frictional resistance [4]. Compared to millimeter bubbles, microbubbles have a large interfacial area concentration and a high mass transfer rate due to the large internal pressure, as well as having high penetration ability into narrow areas [5]. In addition to these characteristics, microbubble flows can be composed of only gases and water, making them economical and low environmental impact, and are used in a wide range of fields, such as chemistry [6], agriculture [7], medical [8], water treatment [9-12] and washing process [13].

The cleaning process is important in the manufacturing and production processes of industrial products, and in the food industry the removal of oil and grease from pipes is also necessary [14]. However, conventional industrial cleaning uses chlorofluorocarbon gas, volatile organic compounds, acid-alkali cleaning agents, and other chemicals, which pose environmental burdens and waste liquid treatment costs. There is therefore a need to develop cleaning technologies with less environmental impact.

There have been many studies on cleaning using microbubbles. Lin et al. [15] used microbubbles to remove dental plaque in order to reduce a risk of periodontal disease. Takahashi et al. [16] reported that the use of ozone microbubbles generated by a pressurized dissolution method increased the concentration of ozonized water and improved the cleaning speed, but the cleaning efficiency was inferior to that of hot concentrated sulfuric acid, and the method has not yet been widely put to practical use. Matsuura et al. [17] carried out cleaning of polymer ink from a glass substrate using microbubbles. They suggested that the cleaning method should take into account

microbubble adsorption onto ink surfaces to improve the cleaning effects on hydrophobic materials. Factors that make water containing microbubbles effective for cleaning have been speculated as adsorption of dirt at the gas-liquid interface, an effect of surface charge, an abrasive effect of bubbles, a lifting effect of dirt by bubbles and so on [18]. However, none of the factors has been clearly demonstrated, and the detailed mechanisms related to the removal effect have not been fully elucidated.

It is important to develop a measurement method to quantitatively evaluate the cleaning effect to clarify the cleaning process with microbubbles. Akuzawa et al. [19] proposed a method for continuously measuring the amount of removed lard oil based on temporal changes in the intensity of fluorescence generated by irradiation of a laser beam to the lard oil mixed with fluorescent dye (laser-induced fluorescence method). Although this method enables them to quantitatively evaluate the amount of removed oil, the effects of microbubbles on the oil-removal process could not be discussed in detail due to lack of the information on the microbubble characteristics such as the number density and the diameter.

In this study, experiments on the removal effects of water flows in a horizontal channel with and without microbubbles were conducted to investigate the oil removal process with microbubbles. Silicone oil adhering to the bottom wall of the channel was used as dirt. The local thickness of the oil was measured during cleaning from micrographs of fluorescence intensity from fluorescent dye mixed into the oil. The bubble diameter and number density in the vicinity of the oil were also measured by using an image processing method. The behavior of microbubbles in the vicinity of the oil and its relation with the removal process were also discussed.

2. Experimental apparatus and methods

2.1. Observation system and experimental condition

Fig. 1 (a) shows a schematic of the experimental apparatus which consisted of a microbubble generator (Science, SMBO-PS480), an acrylic water tank, a pump (IWAKI, MD-6ZK), a flow meter (Nippon Flow Cell, NSP-5-B006), a test section, and an inverted microscope (Nikon, ECLIPSE Ti-U). The dimensions of the tank were 300 × 300 × 500 mm in width, depth and height, respectively. The tank was filled with water purified using a water purification system (Merck, Elix UV5). The water temperature T [K] and the dissolved oxygen concentration DO [kg/m^3] in the water tank were measured using a waterproof digital thermometer (Nekken, Safety Thermo, SN3000) and a luminescent dissolved oxygen meter (HACH HQ30d LDO101-01), respectively. The temperature was T = 298 ± 0.5 K and DO of purified water was (8.45 ± 0.2) × 10^{-3} kg/m^3. During the experiment with flows containing microbubbles, the microbubble generator was operated for a sufficient time in advance to reach a quasi-equilibrium state in the tank, DO at which was (9.25 ± 0.2) × 10^{-3} kg/m^3. Water was then started to flow into the channel by the pump. After passing through the test section, water flowed into a drain tank. The liquid volume flow rate was adjusted using valves installed in the flow path.

A cross-section of the oil removal section is shown in **Fig. 1** (b). The measurement section was a part of the bottom surface of the rectangular channel with the cross-sectional area of 5 and 10 mm in height and width, respectively. The area of the oil part was 4 mm × 4 mm and the depth was 200 μm. The bottom plate was removable, and the oil containing fluorescent dye was applied to a recess on the top surface of the protruding part of the bottom plate, which was then fixed in such a way that the oil interface was exposed to the water flow on the same plane as the bottom wall of the channel, i.e., flush

mounted as shown in **Fig. 1** (c). The initial thickness of oil was 200 μm and the change in the thickness could be measured without removing the test section, thereby enabling non-contact and continuous measurement of the oil thickness.

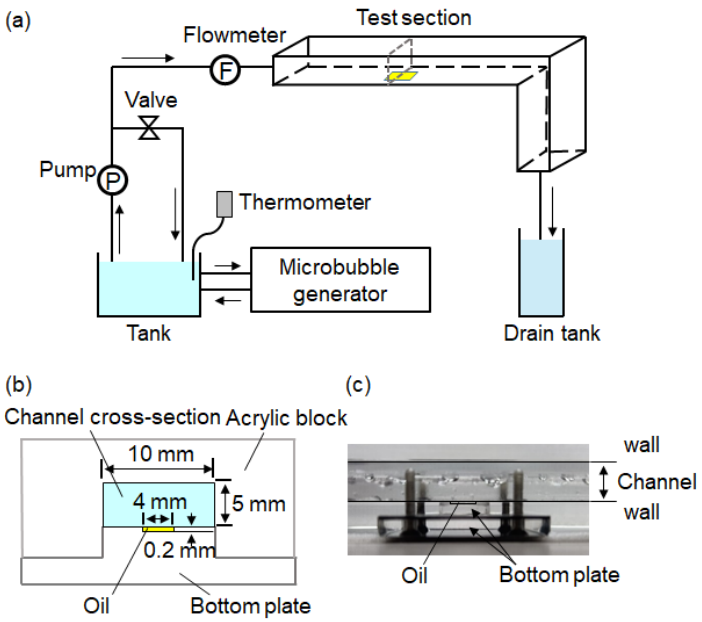

Fig. 1 Experimental apparatus. (a) Schematic of experimental setup. (b) Channel cross-section of test section. (c) Side view of test section.

Fig. 2 shows a schematic of the optical system for observation using an inverted microscope. The test section was set on the stage, a high-speed camera (Photron, FASTCAM NOVA S12) was mounted on the camera port, and the microscope backlight or laser beam was illuminated according to the imaging conditions. The magnification of the objective lens (Nikon, S Plan Fluor 10×) was 10, and the resolution of the captured images was 2 μm/pixel. In the measurements of bubble diameter and bubble number density, the backlight was irradiated from above the test section and the transmitted light was recorded by the high-speed camera.

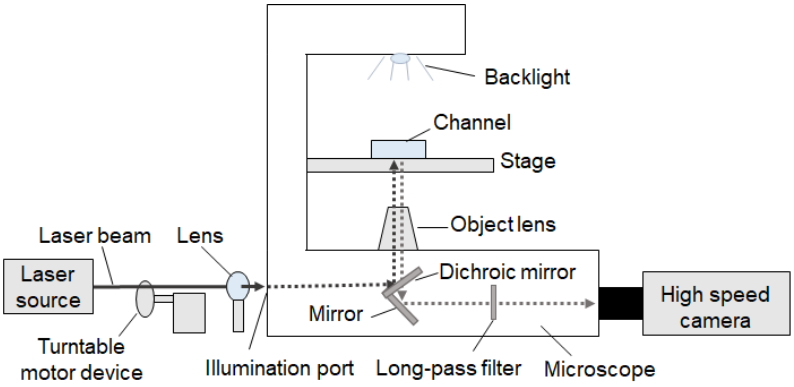

Fig. 2. Optical setup for micrography.

A laser beam was used to irradiate fluorescent dye in the oil for measuring the oil thickness, δ. *Coumarin* 6 (TCI) was used as fluorescent dye. The laser beam passed through a lens (SIGMAKOKI, DLB-26-120PM) placed between the inverted microscope and the laser source (Optic Electronic Co., Ltd.), which expanded the beam diameter at the focal point of the microscope and widened the region of fluorescence intensity measurement. The laser beam then entered the microscope horizontally through an access port located on the back of the microscope and was reflected by a dichroic mirror (Edmund Optics, DICHROIC LONG-PASS 500NM 25.2 × 35.6) installed at a 45-degree angle in the microscope. The laser beam was then irradiated onto the oil region. A rotary shutter was connected to a motor (ORIENTAL MOTOR Co, Ltd, SCM26JA-360) to control the irradiation time of the laser beam, and the speed was adjusted by a speed controller (US2D6-JA-CC). As shown in **Fig. 2**, the fluorescence emitted from the fluorescent dye in the oil by the laser beam passed through a dichroic mirror and a long-pass filter (Edmund Optics, PREC-ISION LONG-PASS 550NM 25MM). The high-speed camera connected to the camera port was used to take the fluorescence images every 30 s for 120 s, and the oil thickness was measured from the fluorescence intensity at each

instant as will be described in Section 2.2. The shutter speed was 1/6000 s and the frame rate was 10 fps when measuring the oil thickness.

After 120 s, the microscope was used with a 4× objective lens (image resolution was 5 μm/pixel) and backlight to observe the removal process for a wider region and the behavior of microbubbles in the vicinity of the oil interface. The shutter speed was 1/16000 s and the frame rate was 10 fps.

The experiments were carried out at Re = 250, 750, 5000 and 6750 so as to observe cleaning effects in laminar and turbulent flows, where Re is the Reynolds number defined by

$$Re = \frac{\rho \bar{u} d_H}{\mu} \tag{1}$$

Here ρ is the density of water (998 kg/m^3), μ is the viscosity of water (0.89 mPa·s), $\bar{u}$ (= Q/S_c) is the cross-sectional mean velocity, d_H (= $4S_c/P_e$) is the hydraulic equivalent diameter, Q is the liquid volume flow rate, S_c is the channel cross-sectional area (50 mm^2), and P_e is the perimeter of the channel (30 mm).

2.2. Image analyses

Fig. 3 shows a grayscale image (300 × 300 pixel) recorded for the oil thickness measurement. The spatial resolution of the image was 2 μm/pixel. The mean fluorescence intensity $\bar{I}$ was obtained by averaging the local intensity (grey scale value), I_{ij}, of each pixel ij, that is

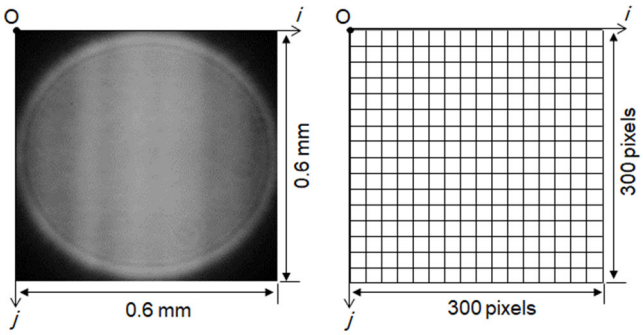

Fig. 3. An example of fluorescence image.

$$\bar{I} = \frac{\sum_{j=0}^{j=299} \sum_{i=0}^{i=299} M_{ij} I_{ij}}{\sum_{j=0}^{j=299} \sum_{i=0}^{i=299} M_{ij}} \tag{2}$$

where M_{ij} is a mask function which takes 1 for fluorescence region and 0 for background region.

When the fluorescence is irradiated with a laser beam, electrons of the fluorescent dye molecules are excited. Photons are emitted when returning from the excited state to the ground state. The number of emitted photons is proportional to the concentration, C, of the fluorescent dye in the sample, δ and the intensity, I_L, of the laser light. The fluorescence intensity, I, can therefore be expressed as

$$I \propto C I_L \delta \tag{3}$$

Two slide glasses (Artec, 8534) were set up as shown in **Fig. 4** (a) for validation of this relation. The gap between the slide glasses was filled with an oil, and the fluorescence intensity was measured by irradiating a laser beam from below. Moving from $\delta = 0.05$

mm to 0.40 mm in 0.05 mm increments, images were taken at each position and the average fluorescence intensities were obtained. The relationship between δ and $\bar{I}$ is shown in **Fig. 4** (b). The linear increase in $\bar{I}$ with increasing δ shows that Eq. (3) is valid.

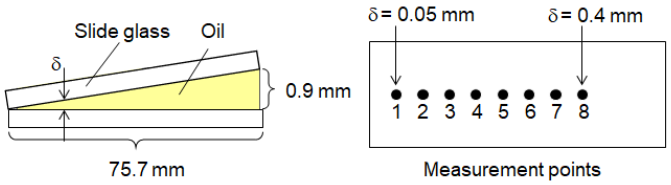

(a) Test cell and measurement points.

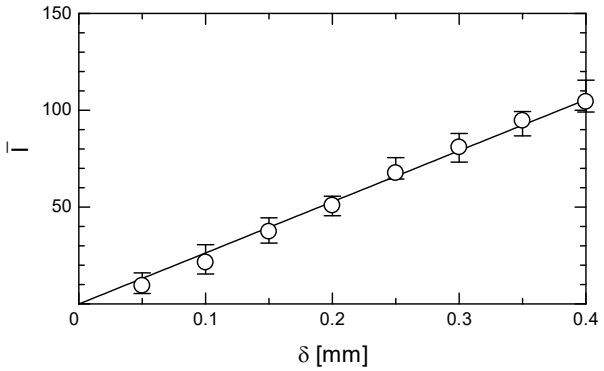

(b) Relation between δ and $\bar{I}$

Fig. 4. Relation between oil thickness δ and fluorescence intensity $\bar{I}$.

It is known that fluorescent dyes exhibit a decrease in fluorescence intensity after prolonged exposure to laser light, i.e., photobleaching [20]. Thus, it is necessary to understand the amount of fluorescence intensity reduction due to photobleaching to evaluate the oil thickness from $\bar{I}$. Fluorescence intensities for photobleaching without flow and for cleaning condition are denoted by $I_P(t)$ and $I_C(t)$, respectively. Since the initial thickness, δ(0), of the sample oil is constant, from Eq. (3), the fluorescence

intensity and initial thickness are related as $I_P(0) = I_C(0) = CI_L\delta(0)$. When confirming the photobleaching effect, the thickness $\delta(t)$ of the oil does not change because of no flow, i.e., $\delta(t) = \delta(0)$. The proportionality between $I_P(t)$ and $\delta(0)$ can therefore be expressed as

$$I_P(t) \propto CI_L\delta(0)f(t) \tag{4}$$

where $f(t)$ is the decay rate of $\bar{I}$ due to photobleaching. In the oil removal experiment, the relationship between $I_C(t)$ and $\delta(t)$ can be expressed as (**Fig. 5**)

$$I_C(t) \propto CI_L\delta(t)f(t) \tag{5}$$

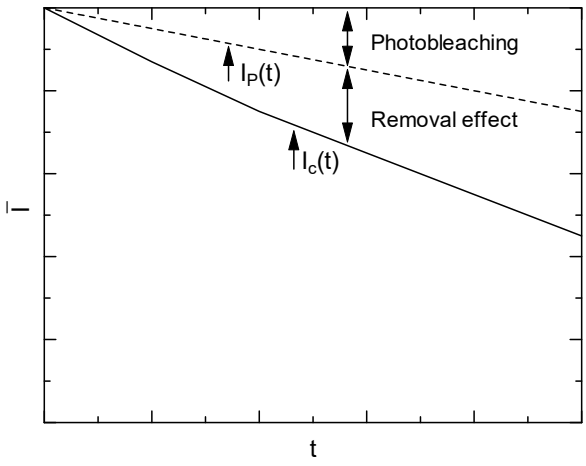

Fig. 5. Relationship between removal effect and photobleaching.

Substituting Eq. (4) into Eq. (5) yields

$$\delta(t) = \frac{I_{\mathrm{C}}(t)}{I_{\mathrm{P}}(t)}\delta(0) \tag{6}$$

The oil thickness can therefore be evaluated from I_{P} and I_{C}.

To reduce the influence by the variation in C and/or I_{L} in each experimental run, the normalized intensities were used:

$$\delta(t) = \frac{I'_{\mathrm{C}}(t)}{I'_{\mathrm{P}}(t)}\delta(0) \tag{7}$$

where $I'_{\mathrm{C}}(t) = I_{\mathrm{C}}(t)/I_{\mathrm{C}}(0)$ and $I'_{\mathrm{P}}(t) = I_{\mathrm{P}}(t)/I_{\mathrm{P}}(0)$. By obtaining $I_{\mathrm{C}}(t)/I_{\mathrm{C}}(0)$ and $I_{\mathrm{P}}(t)/I_{\mathrm{P}}(0)$, the thickness, $\delta(t)$, at each time can be obtained.

The sphere-volume-equivalent diameter, $d_{\mathrm{B}i}$, of each bubble flowing in the vicinity of the oil interface was obtained by image processing [21], where the subscript i is the index of bubbles detected in the images. The geometric centers of the bubbles were detected using the Hough transformation after detecting the contours of bubbles by the Sobel filter and binarization. The diameters of the detected bubbles were evaluated as the mean distances between the centers and the contours. The mean bubble diameter, $\overline{d}_{\mathrm{B}}$, was then calculated as

$$\overline{d}_{\mathrm{B}} = \frac{1}{N}\sum_{i=1}^{N} d_{\mathrm{B}i} \tag{8}$$

where N is the total number of bubbles detected. The number density, $\overline{n}_{\mathrm{B}}$, of

microbubbles was calculated as

$$\bar{n}_{\mathrm{B}} = \frac{1}{HS}\left[\frac{1}{K}\sum_{j=1}^{K} N_{\mathrm{B}j}\right] \tag{9}$$

where K is the number of sample images (20,000), H is the depth of field (DOF, 310 μm), S is the measurement area, and $N_{\mathrm{B}j}$ is the number of bubbles in the jth image. The uncertainty in $\bar{n}_{\mathrm{B}}$ was 5.4×10^6 m^{-3}, which is about 0.8% of the typical value of $\bar{n}_{\mathrm{B}}$.

3. Results and discussion

3.1. Influence of water flow on oil removal

Before discussing the removal effects by a water flow with microbubbles, the influence of water flow is investigated in this section. Two laminar flow conditions (Re = 250 and 750) and two turbulent flow conditions (Re = 5000 and 6750) were considered. **Fig. 6** shows changes in δ until 120 s. The δ decreases with increasing time. The amount of removed oil increases with increasing Re. Therefore, even without microbubbles, the water flow has a removal effect.

The relationship between the thickness decreasing rate, $-d\delta/dt$, and the shear stress, τ_{w}, is shown in **Fig. 7**, where $d\delta/dt$ is calculated by fitting a linear function to the $\delta(t)$ data and τ_{w} is estimated as

$$\tau_{\mathrm{w}} = \frac{1}{2}\frac{\lambda}{4}\rho u^{-2} \tag{10}$$

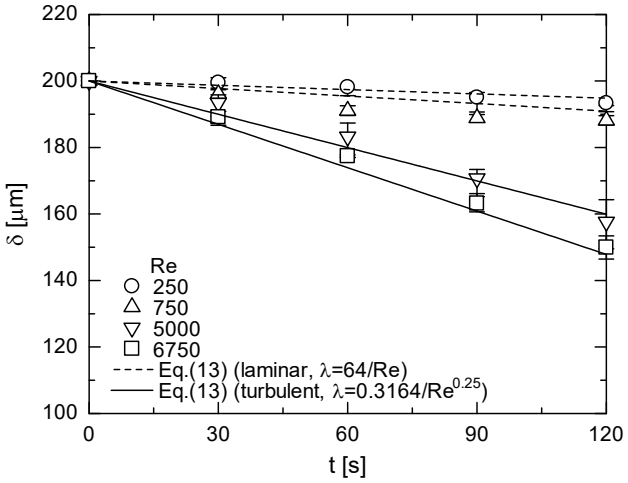

Fig. 6. Changes in oil thickness δ by water flow.

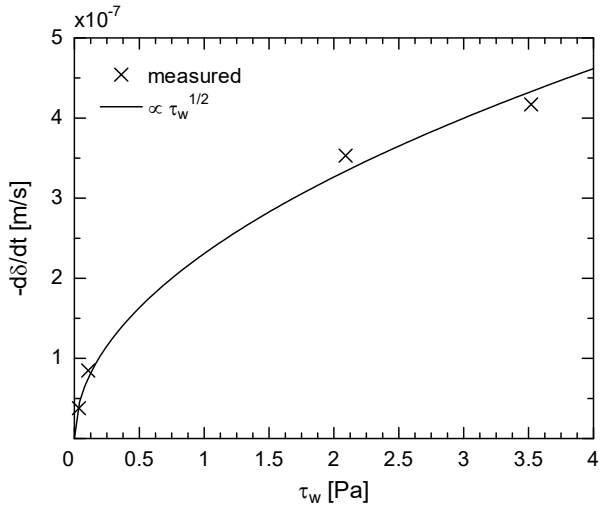

Fig. 7. Relation between $-d\delta/dt$ and τ_w of water flow.

$$\lambda = \begin{cases} 64/Re \ (Re < 2300) \\ 0.3164/Re^{0.25} \ (Re \geq 2300) \end{cases} \tag{11}$$

The removal rate increases as the shear stress increases and is proportional to $\tau_w^{1/2}$. Hence, we assume that the removal rate is proportional to the frictional velocity, $u^* = (\tau_w/\rho)^{1/2}$, i.e.

$$\frac{d\delta}{dt} = -c_s\sqrt{\frac{\tau_w}{\rho}} \tag{12}$$

where c_s is a dimensionless constant and its value was obtained as 7.3×10^{-6} by fitting Eq. (12) to the data. Integrating Eq. (12) yields

$$\delta(t) = \delta(0) - c_s\sqrt{\frac{\lambda}{8}}\bar{u}t \tag{13}$$

Eq. (13) is compared with the experimental data as shown in **Fig. 6**. The dashed lines are for the laminar flows, and the solid lines are for the turbulent flows. The correlation is consistent with the experiment. Hence, the oil removal by water flow is mainly due to the shear stress acting on the oil interface.

3.2. Influence of microbubbles on oil removal

Fig. 8 shows the probability density functions (PDFs) of d_B of bubbles within the region from the channel wall to 170 μm apart from the wall. The bin width was set to 5 μm. In all the conditions, the peak diameter around 20 μm slightly decreases as *Re* increases, implying that small microbubbles are brought to the near wall region against buoyancy due to turbulent fluctuations. The effects of *Re* on $\bar{d}_B$ and $\bar{n}_B$ are shown in **Fig. 9**. Increasing *Re* has no significant effect on $\bar{d}_B$ and $\bar{d}_B \sim 30\mu m$. On the other hand, $\bar{n}_B$ increases as *Re* increases.

Fig. 10 shows $\delta(t)$ in water flows with microbubbles. The δ decreases with time, and the amount of removed oil increases with increasing *Re* as well as in the water flow cases. **Table 1** shows δ at 120 s in each case. The removal effects were confirmed to be enhanced

by microbubbles whatever the Reynolds number is.

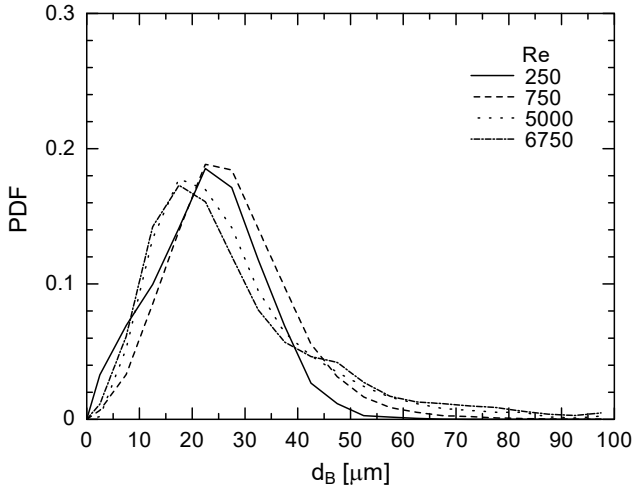

Fig. 8. Probability density function of bubble diameter.

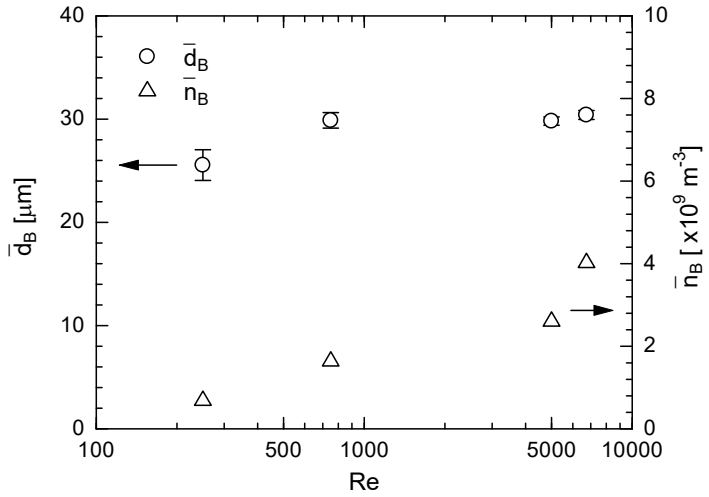

Fig. 9. Relation between *Re* and $\bar{d}_B$, $\bar{n}_B$ of microbubbles.

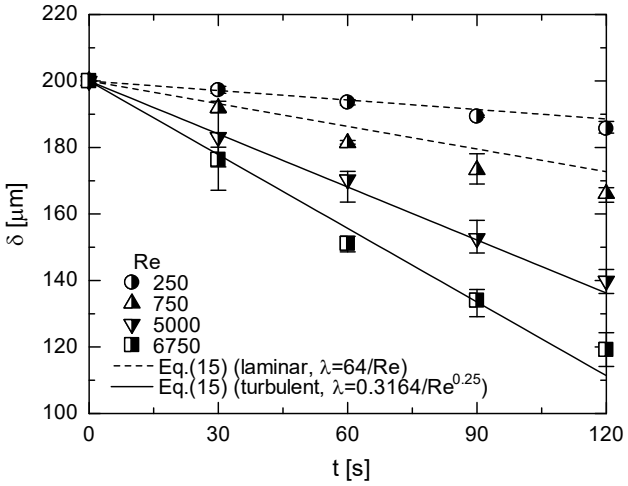

Fig. 10. Changes in oil thickness δ by water flow with microbubbles.

Table 1 Oil thickness at 120 s.

Re	250	750	5000	6750
Water flow	194 μm	188 μm	158 μm	149 μm
Microbubbles flow	186 μm	168 μm	136 μm	114 μm

Fig. 11 shows a relation between $\bar{n}_B$ and the removal rate excluding the effects of water flow, i.e., Eq. (12). It is shown that the effects of microbubbles increase almost linearly as $\bar{n}_B$ increases. Therefore,

$$\frac{d\delta}{dt} = -c_s\sqrt{\frac{\tau_w}{\rho}} - c_B L\bar{n}_B \tag{14}$$

where L is the distance from the oil interface, bubbles within which contribute to oil removal enhancement, and c_B [m^3/s] is a constant representing the amount of oil volume removed by a bubble. The L is approximated as $L \sim \bar{d}_B$, so that

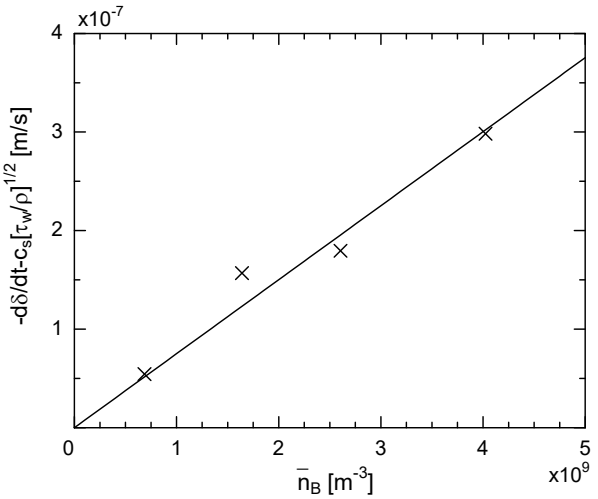

Fig. 11. Relation between $-d\delta/dt - c_s[\tau_w/\rho]^{1/2}$ and $\bar{n}_B$ of water flow.

$$\delta(t) = \delta(0) - \left(c_s \sqrt{\frac{\lambda}{8}} \bar{u} + c_B \bar{d}_B \bar{n}_B \right) t \tag{15}$$

By fitting this functional form to the data, we obtained $c_B = 3.8 \times 10^{-12}$ m^3/s. Eq. (14) is compared with the data in **Fig. 10**, in which the dashed lines are for the laminar flow cases and the solid lines are for the turbulent flow cases. The data and the correlation are in reasonable agreement, which demonstrates the validity of the model.

3.3. Adhesion of microbubbles on oil interface under turbulent flow condition

In the above sections, the removal effect was locally evaluated using the laser-induced fluorescence. In the microbubble experiment, the fluorescence intensity $\bar{I} = 0$ occurred after $t = 240$ s in the turbulent flow of $Re = 6750$. **Fig. 12** shows the process of oil removal. Microbubbles attach to the water-oil interface and the number of adhering bubbles increases as t increases. The bubble size obviously becomes large. The large bubble indicated with the white circle at $t = 330$ s is swept away by the water flow in the direction

of the black arrow. After that, peel-off indicated with the black dashed circle occurs from the original location of the large bubble. The peeling also expands with t in the direction of the white arrow shown in the image of t = 480 s. **Fig. 13** shows the process of large bubble generation, where t' is the time at which the bubbles attach to the oil interface and get larger. The state of microbubble adhesion and growth is shown in **Fig. 13** (a). Large bubbles coming from the upstream could not attach to oil, and only microbubbles did due to turbulent fluctuations. In addition, the attached microbubbles became larger and coalesced with other bubbles around them as shown in **Fig. 13** (b). The coalescence of such bubbles resulted in bubbles reaching a certain degree of size, and they were pushed and swept away by the water flow, followed by peel-off.

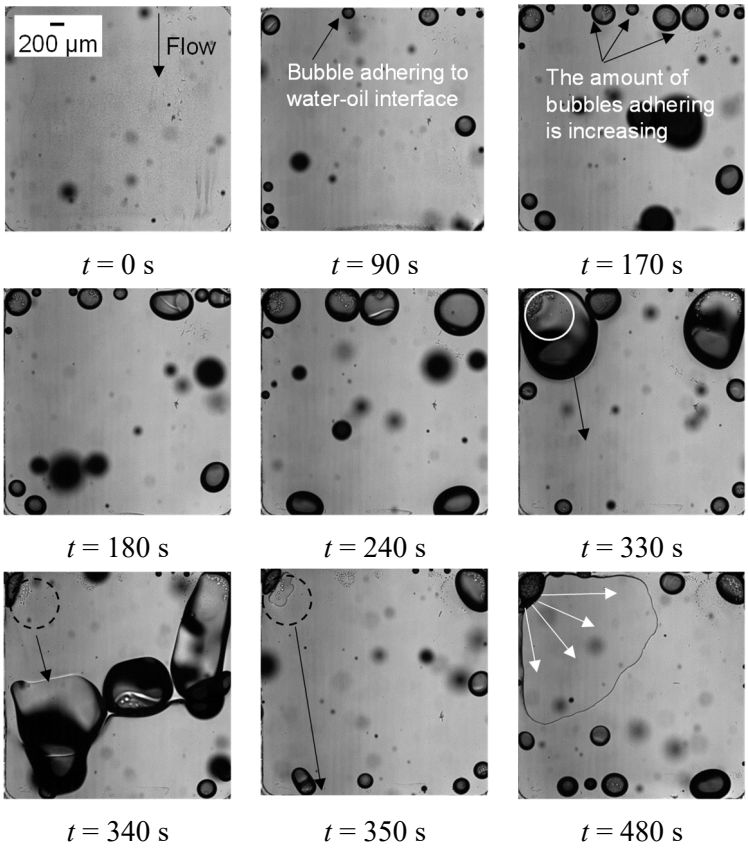

Fig. 12. Processes of oil removal with bubble detachment (Re = 6750).

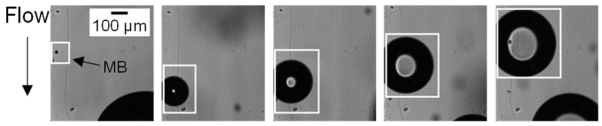

t' = 0 s 60 s 120 s 180 s 240 s

(a) Microbubble attachment and get larger in oil.

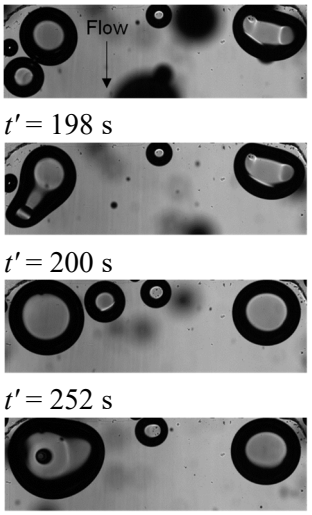

t' = 198 s

t' = 200 s

t' = 252 s

t' = 267 s

(b) Bubble coalescence.

Fig. 13. Microbubble attachment in oil and bubble coalescence.

Let us check whether the growth of microbubbles is caused by coalescence or mass transfer of gaseous species from water to the bubbles. Water with microbubbles was made to flow into the channel, and then we stopped the water flow immediately after some microbubbles attached to the oil. This condition is referred to as the stagnant water condition in the following. The relationship between d_B and t' in the stagnant water condition is shown in **Fig. 14**; microbubbles can grow by mass transfer of oxygen from water without coalescing with each other. A relation between d_B and t' in water flow is also shown in **Fig. 14**. In the microbubble flow, DO in the tank was kept at 9.25×10^{-3} kg/m^3 due to the continuous generation of microbubbles. That is, it provided the same

DO in the vicinity of the oil, regardless of time. The growth rate in the bubbly flow was the same as in the stagnant water at the initial growth stage and, thus, microbubbles in the presence of water flow also grew by mass transfer without coalescing. After 90 s, the microbubbles in the bubbly flow grew faster after a certain time if no coalescence occurred in the bubbly flow. The data of the microbubble flow in **Fig. 14** departs from those of the stagnant flow case after 120 s. This is due to bubble coalescence with surrounding bubbles. The bubble size became larger than 300 mm and coalesced with another large bubble as shown in **Fig. 15**, which causes the jump in the data plots at 240 s.

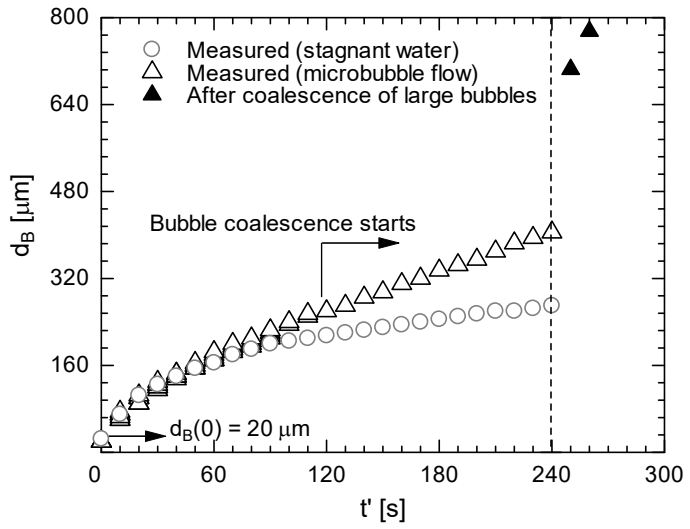

Fig. 14. Relation between d_B and t' in stagnant water and microbubbles flow.

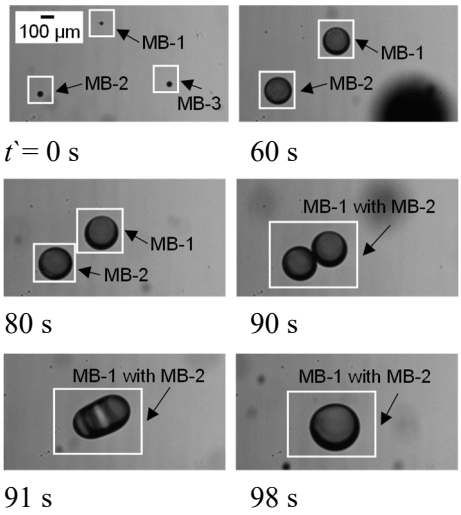

Fig. 15. Microbubbles (MB) grow to a certain degree and coalesce with other bubbles.

It is important to observe the condition under which the peeling occurs and to evaluate the extent of the peeling. **Fig. 16** (a) shows the state of oil at t = 600 s in water flow of Re = 750 with microbubbles. The fluorescence intensity measurement showed the decrease in thickness under this condition, but no peel-off was observed. The black shading regions in the image indicate bubbles in water and on the upper wall of the channel outside the focal plane. In this experiment, the microbubbles did not adhere to the interface, resulting in no peeling in the laminar flow even with microbubbles. **Fig. 16** (b) shows oil images in the turbulent flow of Re = 6750 without microbubbles at t = 600 s and 720 s. No peeling was observed in these flows. **Fig. 16** (c) shows the state of oil in turbulent flow with microbubbles. At t = 600 s, peeling of oil occurred and the area of peeling expanded with time. **Fig. 17** shows the ratio of the area, in which peel-off takes place, to the area of oil region (4 mm x 4 mm). Peeling began around t = 380, and the peel-off rate increased with time. Note that the increase in the mean water velocity by the decrease in the cross-sectional area due to the presence of bubbles adhering to the oil region is small and does not give a remarkable increase in the viscous shear stress at the

oil interface. The removal rate by peeling is much larger than that by water flow; therefore, the peeling effect is dominant in the removal rate at the later stage of cleaning under the turbulent flow condition.

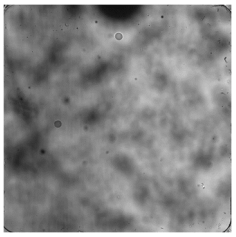

t = 600 s

(a) Microbubbles flow in laminar flow (Re = 750).

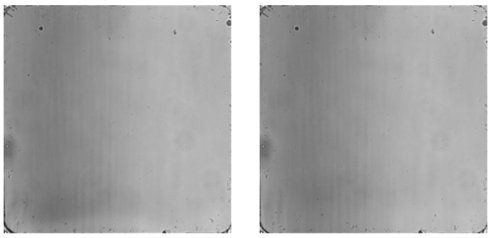

t = 600 s t = 720 s

(b) Water flow in turbulent flow (Re = 6750).

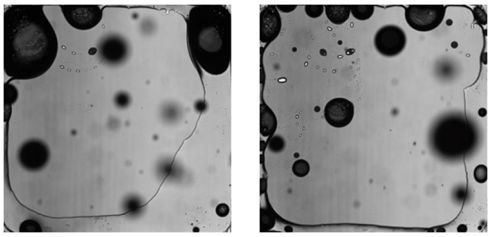

t = 600 s t = 720 s

(c) Peel-off of microbubbles flow in turbulent flow (Re = 6750).

Fig. 16. Microbubble adhesion and peel-off.

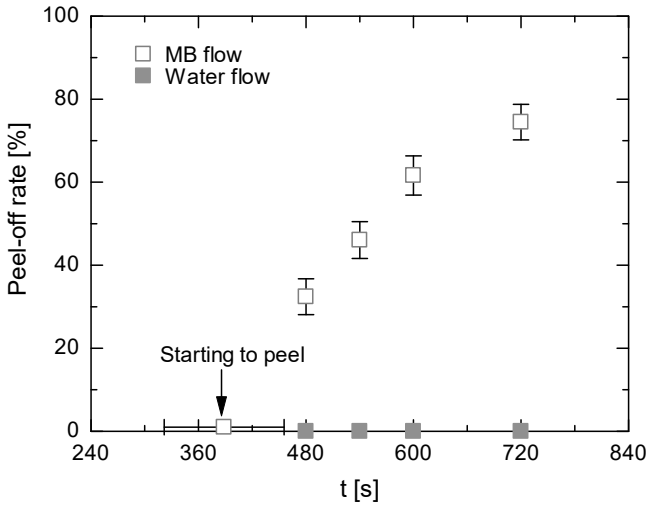

Fig. 17. Relation between peel-off rate and t (Re = 6750).

Fig. 18 shows a schematic of the whole process of oil removal. In the early stage (the left part of the figure), oil removal is mainly due to the shear stress acting on the oil interface, and when microbubbles are mixed, the microbubble effect is superposed. In a turbulent bubbly flow at high Re, microbubbles attach to the water-oil interface, and those bubbles grow by mass transfer of gas species from water and the bubble growth initiates bubble coalescence from $t \sim 120$ s. Bubbles that have grown by bubble coalescence are swept away by the water flow, which results in peel-off around $t = 380$ s (the right part of the figure). The overall residual adhering rate decreases with time.

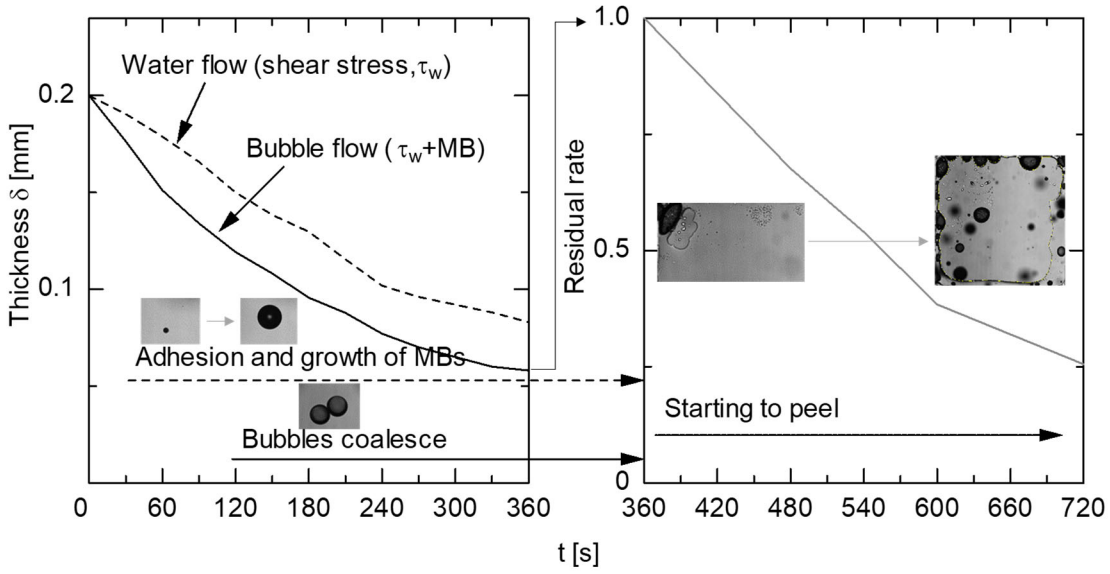

Fig. 18. The process of removing oil by water flow with microbubble (turbulent).

4. Conclusions

Oil removal experiments were conducted using viscous silicone oil adhering to the bottom wall of a horizontal rectangular channel to investigate the effects of microbubbles on the removal of oil on the wall surface. The fluorescence intensity of the fluorescent dye mixed in the silicone oil was photographed by a microscope to measure the change in oil thickness, and the bubble diameter and number density in the vicinity of the wall surface were also measured to investigate the removal rate enhanced by microbubbles. As a result, the following conclusions were obtained:

(1) The amount of oil removed by the water flow increases with increasing *Re*, showing that the water flow has cleaning effects even without microbubbles. This is attributed to the shear stress acting on the oil interface.

(2) Adding microbubbles to the water flow increases the amount of oil removal. In other words, microbubbles have a removal enhancement effect. The higher the bubble

number density, the larger the removal effect is. The removal effect of microbubbles can be evaluated by a model that assumes that the amount of oil removal is proportional to the number of microbubbles in the vicinity of oil interface.

(3) The removal rate can be modeled as a superposition of the effects of shear stress and the presence of microbubbles.

(4) Microbubbles adhering to oil under turbulent conditions can grow by mass transfer. The cleaning effect is largely promoted by peeling of the oil due to the detachment of large bubbles grown on the oil interface.

References

[1] ISO 20480-1:2017 Fine bubble technology — General principles for usage and measurement of fine bubbles — Part 1: Terminology.

[2] M. Takahashi, K. Chiba, P. Li, Free-Radical Generation from Collapsing Microbubbles in the Absence of a Dynamic Stimulus, *J. Phys. Chem. B* 111 (2007) 1343–1347.

[3] K. Tan, Y. Mohan, K. Liew, S. Chong, P. Poh, Development of an effective cleaning method for metallic parts using microbubbles, *J. Clean. Prod*. 261 (2020) 121076.

[4] Y. Feng, H. Hu, G. Peng, Y. Zhou, Microbubble effect on friction drag reduction in a turbulent boundary layer, *Ocean Eng.* 211 (2020) 107583.

[5] S. Tanaka, S. Kastens, S. Fujioka, M. Schlüter, K. Terasaka, Mass transfer from freely rising microbubbles in aqueous solutions of surfactant or salt, *Chem. Eng. J.* 387 (2020) 121246.

[6] M. Matsumoto, T. Fukunaga, K. Onoe, Polymorph control of calcium carbonate by reactive crystallization using microbubble technique, *Chem. Eng. Res. Des.* 88 (2010) 1624–1630.

[7] Y. Liu, Y. Zhou, T. Wang, J. Pan, B. Zhou, T. Muhammad, C. Zhou, Y. Li, Micro-nano bubble water oxygation: Synergistically improving irrigation water use efficiency, crop yield and quality, *J. Clean. Prod.* 222 (2019) 835–843.

[8] Y. Kaneko, T. Maruyama, K. Takegami, T. Watanabe, H. Mitsui, K. Hanajiri, H. Nagawa, Y. Matsumoto, Use of a microbubble agent to increase the effects of high intensity focused ultrasound on liver tissue, *Eur. Radiol*. 15 (2005) 1415–1420.

[9] L. B. Chu, X. H. Xing, A. F. Yu, X. L. Sun, B. Jurcik, Enhanced treatment of practical textile wastewater by microbubble ozonation, *Process Saf. Environ. Prot.* 86 (2008)

389–393.

[10] W. Zhang, F. Jiang, Membrane fouling in aerobic granular sludge (AGS)-membrane bioreactor (MBR): Effect of AGS size, *Water Res.* 157 (2019) 445–453.

[11] S. Meng, X. Meng, W. Fan, D. Liang, L. Wang, W. Zhang, Y. Liu, The role of transparent exopolymer particles (TEP) in membrane fouling: A critical review, *Water Res.* 181 (2020) 115930.

[12] W. Zhang, W. Liang, Z. Zhang, T. Hao, Aerobic granular sludge (AGS) scouring to mitigate membrane fouling: Performance, hydrodynamic mechanism and contribution quantification model, *Water Res.* 188 (2021) 116518.

[13] C. Oliveira, R. T. Rodrigues, J. Rubi, A new technique for characterizing aerated flocs in a flocculation-microbubble flotation system, *Int. J. Miner. Process* 96 (2010) 36–44.

[14] S. Liu, Q. Wang, H. Ma, P. Huang, J. Li, T. Kikuchi, Effect of micro-bubbles on coagulation flotation process of dyeing wastewater, *Sep. Purif. Technol*. 71 (2010) 337–346.

[15] P. J. Lin, M. C. Chuang, S. C. Chang, Research on the cleaning efficacy of micro-bubbles on dental plaque, *Procedia Manuf*. 3 (2015) 13–20.

[16] M. Takahashi, H. Ishikawa, T. Asano, H. Horibe, Effect of Microbubbles on Ozonized Water for Photoresist Removal, *J. Phys. Chem. C* 116 (2012) 12578–12583.

[17] K. Matsuura, S. Ogawa, S. Kasaki, K. Koyama, M. Kodama, S. Yanase, Cleaning polymer ink from a glass substrate using microbubbles generated by a hydrogen bubble method, *Sep. Purif. Technol*. 142 (2015) 242–250.

[18] I. D. Sta Maria, M. W. Lim, E. V. Lau, Multiple roles of graphene nanoparticles

(GNP) in microbubble flotation for crude oil recovery from sand, *Results in Engineering* 11 (2021) 100271.

[19] H. Akuzawa, K. Amagai, M. Funatsu, F. Takakusagi, K. Tabei, Y. Noda, Study on cleaning of pipe inner wall by micro-bubble flow (in Japanese), *Japanese J. Multiphase Flow* 24 (2010) 454–461.

[20] S. Khandai, R. A. Siegel, S. S. Jena, Probing the microenvironment of polyacrylamide hydrogel matrix using turbidity and fluorescence recovery after photobleaching: One versus Two phases, *Colloids Surf. A Physicochem. Eng. Asp.* 593 (2020) 124618.

[21] Y. Li, S. Hosokawa, K. Hayashi, A. Tomiyama, N. Shibata, Y. Maeda, generation of microbubbles by subcooled boiling of water with dissolved incondensable gases, *Multiph. Sci. Technol*. 33 (2021) 17–31.

List of tables

Table 1 Oil thickness at 120 s.

Re	250	750	5000	6750
Water flow	194 μm	188 μm	158 μm	149 μm
Microbubbles flow	186 μm	168 μm	136 μm	114 μm

Figure captions

Fig. 1. Experimental apparatus. (a) Schematic of experimental setup. (b) Channel cross-section of test section. (c) Side view of test section.

Fig. 2. Optical setup for micrography.

Fig. 3. An example of fluorescence image.

Fig. 4. Relation between oil thickness δ and fluorescence intensity $\bar{I}$. (a) Test cell and measurement points. (b) Relation between δ and $\bar{I}$.

Fig. 5. Relationship between removal effect and photobleaching.

Fig. 6. Changes in oil thickness δ by water flow.

Fig. 7. Relation between $-d\delta/dt$ and τ_w of water flow.

Fig. 8. Probability density function of bubble diameter.

Fig. 9. Relation between *Re* and $\bar{d}_B$, $\bar{n}_B$ of microbubbles.

Fig. 10. Changes in oil thickness δ by water flow with microbubbles.

Fig. 11. Relation between $-d\delta/dt - c_s[\tau_w/\rho]^{1/2}$ and $\bar{n}_B$ of water flow.

Fig. 12. Processes of oil removal with bubble detachment (*Re* = 6750).

Fig. 13. Microbubble attachment in oil and bubble coalescence. (a) Microbubble attachment and get larger in oil. (b) Bubble coalescence.

Fig. 14. Relation between d_B and t' in stagnant water and microbubbles flow.

Fig. 15. Microbubbles (MB) grow to a certain degree and coalesce with other bubbles.

Fig. 16. Microbubble adhesion and peel-off. (a) Microbubbles flow in laminar flow (*Re* = 750). (b) Water flow in turbulent flow (*Re* = 6750). (c) Peel-off of microbubbles flow in turbulent flow (*Re* = 6750).

Fig. 17. Relation between peel-off rate and *t* (*Re* = 6750).

Fig. 18. The process of removing oil by water flow with microbubble (turbulent).